ACS APPLIED MATERIALS & INTERFACES

Research Article

www.acsami.org

UV-Enhanced NO_2 Gas Sensing Properties of SnO_2-Core/ZnO-Shell Nanowires at Room Temperature

Sunghoon Park, Soyeon An, Youngho Mun, and Chongmu Lee*

Department of Materials Science and Engineering, Inha University, 253 Yonghyun-dong, Nam-gu, Incheon 402-751, Republic of Korea

Supporting Information

ABSTRACT: SnO_2-core/ZnO-shell nanowires were synthesized using a two-step process: the synthesis of SnO_2 nanowires by the thermal evaporation of Sn powders followed by the atomic layer deposition of ZnO. The room temperature NO_2 gas sensing properties of the nanowires under ultraviolet (UV) illumination were examined. The cores and shells of the nanowires were primitive tetragonal-structured single crystal SnO_2 and wurtzite-structured single crystal ZnO, respectively. The responses of multiple networked SnO_2 nanowire sensors were increased 2−3-fold at NO_2 concentrations ranging from 1 to 5 ppm by encapsulating the nanowires with ZnO. The SnO_2-core/ZnO-shell nanowire sensors showed a remarkably enhanced response under UV illumination. The sensing mechanism of the core/shell nanowires under UV illumination is also discussed.

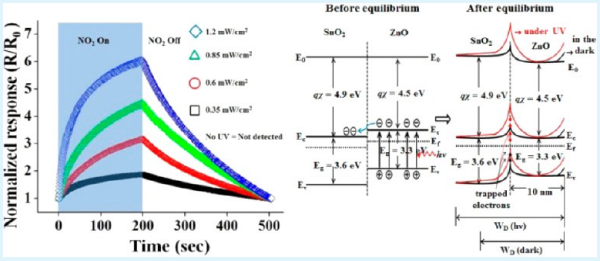

KEYWORDS: *SnO_2, ZnO, core/shell nanowires, gas sensor, UV irradiation*

1. INTRODUCTION

In recent years, semiconducting oxide nanostructure-based sensors have become a focus of intense research because of their high sensitivity, small size, and low cost.[1−5] On the other hand, semiconducting oxide sensors need to operate at high temperatures of 100−400 °C to achieve excellent sensing performance. In addition to their high power consumption, high temperature operation can result in ignition of flammable and explosive gases. Moreover, high temperature operations can lead to long-term reliability problems due to the growth of oxide grains. A range of techniques such as doping of novel metals,[6−8] microelectromechanical systems (MEMS) fabrication,[9] nanosensing materials,[10] application of an electrostatic field,[11] and ultraviolet (UV) illumination[12−20] have been developed to lower the operating temperature of these sensors. Of these techniques, UV illumination has attracted increasing attention as a promising strategy. Since Camagni et al. reported UV-enhanced gas sensing properties of indium oxide and tin dioxide sensors in 1996,[12] there have been many reports showing that UV irradiation enables sensors to operate at room temperature.[12−20] On the other hand, there are no reports of the effects of the UV illumination intensity on the sensor sensitivity or optimization of the UV illumination intensity.

SnO_2 and ZnO are the two most commonly used materials for gas sensors, but they have shortcomings such as poor selectivity and reliability because they react with several gases simultaneously. SnO_2/ZnO or ZnO/SnO_2 heterostructure formation has been proposed as a potential solution to this problem.[20−25] This paper reports the synthesis of SnO_2-core/ZnO-shell nanowires via a two-step method: the thermal evaporation of Sn powders followed by the atomic layer deposition (ALD) of ZnO. The enhanced room temperature sensing properties of the multiple networked SnO_2-core/ZnO-shell nanowire sensors under UV illumination were investigated. In particular, the effects of the UV illumination intensity on the response of SnO_2-core/ZnO-shell nanowire sensors to NO_2 gas were examined.

2. EXPERIMENTAL SECTION

SnO_2-core/ZnO-shell nanowires were synthesized using a two-step process: synthesis of SnO_2 nanowires by the thermal evaporation of Sn powders followed by the ALD of ZnO. SnO_2 nanowires were grown on Si substrates coated with a 3 nm thick Au thin film by thermal evaporation. Approximately 1.2 g of Sn powders, as starting material, was placed in an alumina crucible and positioned at the center of a horizontal quartz tube. The quartz tube was mounted inside a conventional horizontal tube furnace. During nanowire synthesis, the temperature of the source materials was maintained at 900 °C for 1 h, whereas that of the Au-coated Si substrates was maintained at 700 °C in an N_2/O_2 atmosphere at N_2 and O_2 flow rates of 300 and 10 standard cubic centimeters per minute (sccm), respectively. The pressure in the reactor was kept at 1 Torr. After synthesis, the furnace was cooled to room temperature and the substrates were removed from the tube. Subsequently, the SnO_2 nanowires were transferred to an ALD chamber and coated with ZnO by ALD for 50 cycles. Diethylzinc (DEZn) and H_2O were kept in bubblers at 0 and 10 °C, respectively. The source gases were fed alternately into the chamber through separate inlet lines and nozzles. Typical ALD pulse lengths were 0.15 s for DEZn (0 °C), 0.2 s for H_2O (10 °C), and 3 s for purging

Received: February 6, 2013
Accepted: April 29, 2013
Published: April 29, 2013

the reactants. The substrate temperature and pressure in the chamber were 150 °C and 0.1 Torr, respectively.

The nanowire samples collected were characterized by scanning electron microscopy (SEM, Hitachi S-4300SE), transmission electron microscopy (TEM, JEOL JEM-2100F) equipped with an energy-dispersive X-ray spectrometer (EDXS), and X-ray diffraction (XRD, Philips X'Pert Pro MRD). The crystallographic structure was determined by glancing angle XRD using Cu Kα radiation (0.154 nm) at a scan rate of 2°/min. The sample was arranged geometrically at a 0.5° glancing angle using a rotating detector.

For the sensing measurements, Ni (~10 nm in thickness) and Au (~50 nm) thin films were deposited sequentially by sputtering to form electrodes using an interdigital electrode (IDE) mask. Multiple networked SnO_2-core/ZnO-shell nanowire gas sensors were fabricated by pouring a few drops of nanowire-suspended ethanol onto thermally oxidized Si/SiO_2 substrates equipped with a pair of IDEs with a gap length of 20 μm. The electrical and gas sensing properties of the as-synthesized SnO_2 nanowires and SnO_2-core/ZnO-shell nanowires were measured using a home-built computer-controlled characterization system consisting of a test chamber, sensor holder, Keithley sourcemeter-2612, mass flow controllers, and a data acquisition system (Figure 1). During the measurements, the nanowire gas sensors were

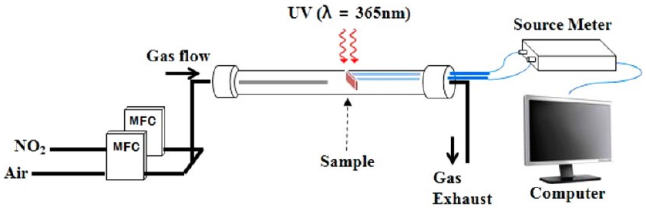

Figure 1. Schematic diagram of the experimental setup.

placed in a sealed quartz tube (test chamber) with a diameter of 45 mm and a length of 800 mm for a volume of ~5087 cm^2 with an electrical feed through. Target gas was prepared by mixing air-base 10 ppm NO_2 gas (purity: 99.999%) with synthetic air (flow rate: 0.5 L/min) to achieve desired concentrations, and the flow rate was maintained at 200 standard cubic centimeter per minute (sccm) using computer-controlled mass flow controllers (MFCs: Kofloc 5400 series; MFC Readout : MR-5000(3.5C Ver.)). The real concentration of the NO_2 target gas prepared finally was measured using a gas detector (model: ToxiRAE-II; maker: RAE system). A National Instruments Labview program was used to control the mass flow controllers and to record the NO_2 concentration. The NO_2 gas passed silica gel to reduce the effects of humidity on the target gas before entering into the chamber through the MFCs, but the level of organic contaminants was not checked before sensing tests. The reference air was introduced to the system through a stainless steel pipe inserted into the quartz tube in a flow mode. The gas was spouted out toward the IDE pattern (or the nanowires) that was attached at the tip of the electrode inserted into the quartz tube on the opposite side of the steel pipe. The distance between the gas outlet and the IDE pattern was ~10 cm. A Keithley sourcemeter-2612 was used to acquire the impedance data. The sourcemeter was hooked to a computer via a GPIB cable, and this data was also acquired using the LabView software. The electrical resistance of gas sensors was determined in the dark and under UV light (λ = 365 nm) illumination at 0.35–1.2 mW/cm^2 by measuring the electric current at room temperature that flowed using a 2612A System Sourcemeter (maker: Keithley) when a potential difference of 1 V was applied between the Ni (~10 nm)/Au (~50 nm) interdigited electrodes. The sampling rate of resistance was 0.5 s/sample. The response of the SnO_2 nanowire sensors is defined as R_g/R_a for NO_2, where R_g and R_a are the electrical resistances of the sensors in target gas and air, respectively.

3. RESULTS AND DISCUSSION

Figure 2a–c shows the SEM images of SnO_2 nanowires, ZnO nanowires, and SnO_2-core/ZnO-shell nanowires synthesized

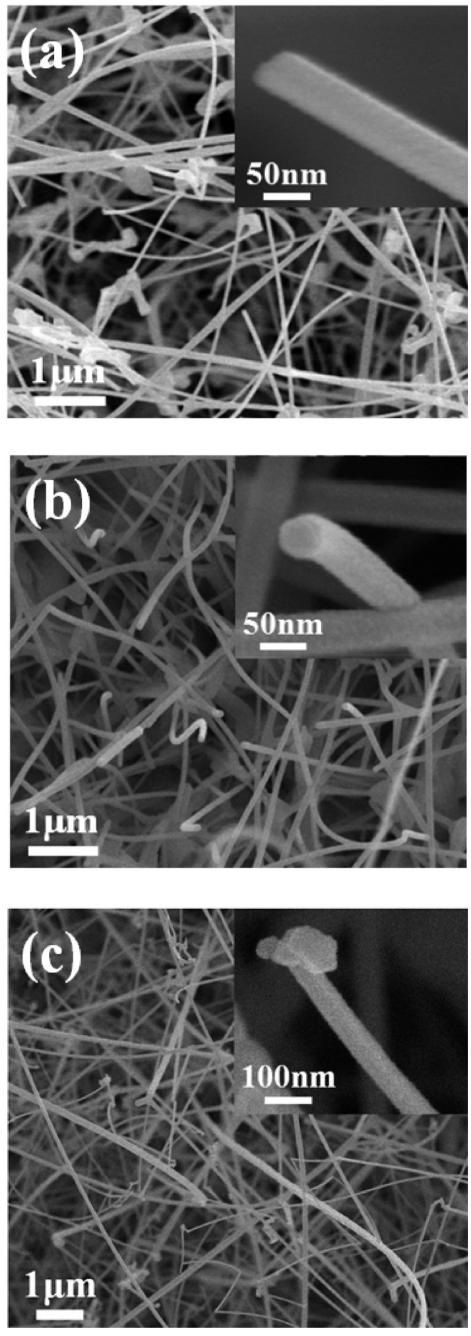

Figure 2. SEM images of (a) SnO_2 nanowires, (b) ZnO nanowires, and (c) SnO_2-core/ZnO-shell nanowires.

in this study. Comparison of their SEM images (Figure 2a–c) and their diameter distributions (Supporting Information, Figure S1) reveal that the diameters of SnO_2 nanowires (d = 68.4 ± 40 nm), ZnO nanowires (d = 72.2 ± 40 nm), and SnO_2-core/ZnO-shell (d = 85.3 ± 40 nm) nanowires were similar each other. Therefore, we may assume that the difference in diameter between different kinds of nanowire sensors will not make any appreciable effect on their sensing results. SnO_2-core/ZnO-shell nanowires with diameters of 50–250 nm and lengths of a few to a few tens of μm were grown using the synthesis scheme adopted in this study. The EDX spectrum of a typical core/shell nanowire (Figure 3a) confirmed that the core/shell nanostructures were composed of Zn, Sn, and O. The Cu in the spectrum was assigned to the TEM grid. A comparison of the EDX spectrum of the central region of a typical

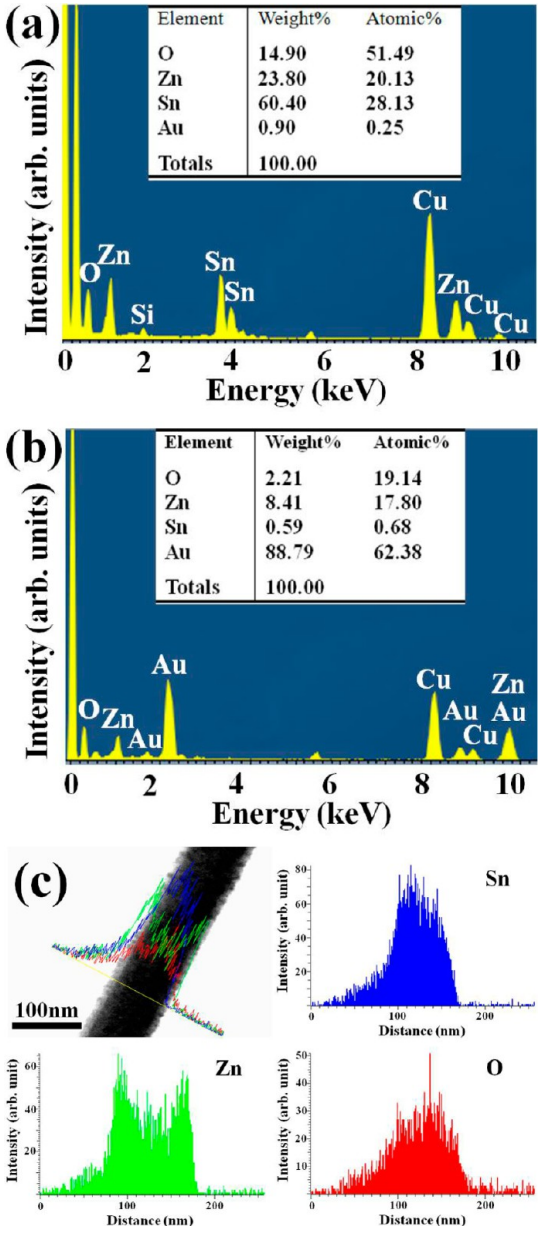

Figure 3. (a) EDX spectrum of the central region of a typical SnO_2-core/ZnO-shell nanowire. (b) EDX spectrum of the tip of core/shell nanowire. (c) EDXS line scanning concentration profiles.

nanowire (Figure 3a) with that focused at the tip of the nanowire (Figure 3b) indicates that the particle at the tip of the nanowire (Figure 2, inset) contained a far higher concentration of Au, suggesting that the nanowire grew via a vapor−liquid−solid mechanism. The line scanning EDXS concentration profile across the diameter of the core/shell nanowires had been synthesized successfully as illustrated by the higher Sn concentration in the central region and higher Zn concentrations at both edge regions of the nanowire.

A low-magnification TEM image of a typical core/shell nanowire revealed a SnO_2 core with a diameter of ∼80 nm at the central region and a ZnO shell with a width of ∼10 nm at the two edge regions of the nanowire (Figure 4a). The enlarged high resolution TEM (HRTEM) image shows fringe patterns in the two different regions, suggesting that both the core and shell are single crystals The resolved spacings between the two

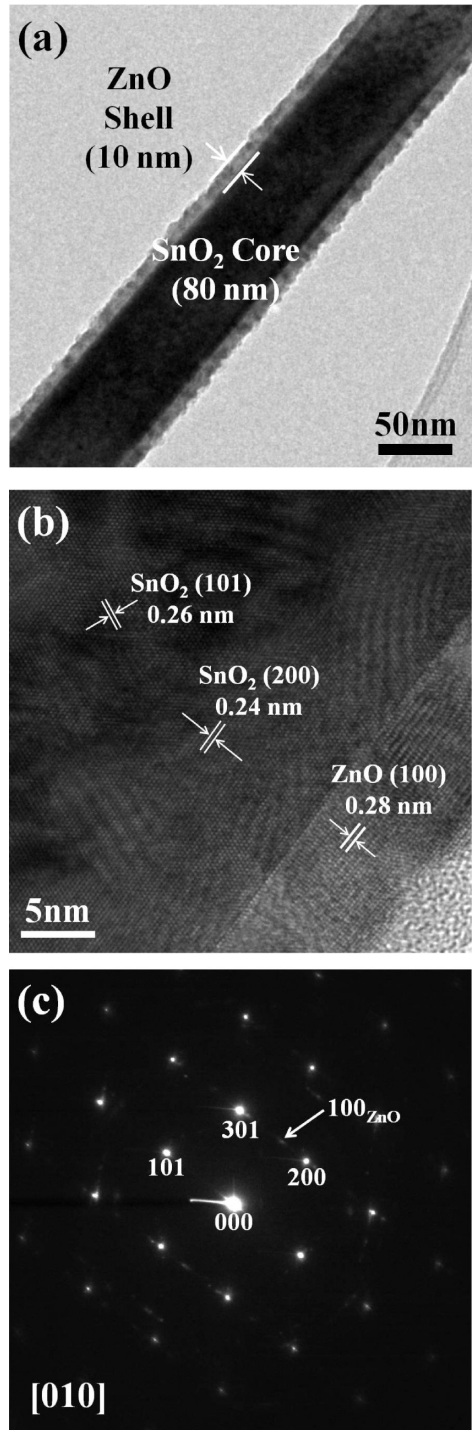

Figure 4. (a) Low magnification TEM image, (b) high-resolution TEM image, and (c) selected area electron diffraction pattern of SnO_2-core/ZnO-shell nanowires.

parallel neighboring fringes were 0.26, 0.24, and 0.28 nm, corresponding to the interplanar spacings of the {101} and {200} lattice planes in tetragonal SnO_2 and the {100} lattice plane in wurtzite ZnO, respectively (Figure 4b). The bright spots in the corresponding selected area electron diffraction (SAED) pattern (Figure 4c) confirmed that both the SnO_2 core and ZnO shell are single crystals. The strong and weak reflection spots were from the SnO_2 core and ZnO shell, respectively.

XRD of SnO_2-core/ZnO-shell nanowires confirmed that both the SnO_2 cores and ZnO shells were single crystals (Figure 5).

dx.doi.org/10.1021/am400500a | ACS Appl. Mater. Interfaces 2013, 5, 4285−4292

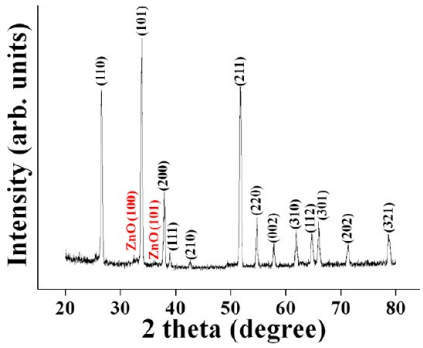

Figure 5. XRD pattern of SnO_2-core/ZnO-shell nanowires.

The main XRD peaks were assigned to the (110), (101), (200), and (111) planes of primitive tetragonal-structured SnO_2 with lattice constants of a = 0.4737 nm and b = 0.3186 nm (JCPDS No. 88-0287). On the other hand, the small reflection peaks, which were so small that they were not nearly noticeable, were assigned to the (100) and (101) planes of wurtzite-type hexagonal structured ZnO with lattice constants of a = 0.3253 nm and c = 0.5213 (JCPDS No. 89-1397).

Figure 6a shows the dynamic responses of pristine SnO_2 nanowires, pristine ZnO nanowires, and SnO_2-core/ZnO-shell nanowires at room temperature to NO_2 gas under UV illumination at 1.2 mW/cm^2. Figure 6b–d presents the enlarged parts of the data in Figure 6a measured at a NO_2 concentration of 5 ppm for pristine SnO_2 nanowires, pristine ZnO nanowires, and SnO_2-core/ZnO-shell nanowires, respectively, showing the moments of gas input and gas stop. The resistance increased upon exposure to NO_2 and recovered completely to the initial value upon the removal of NO_2. The sensor responses to NO_2 gas were also stable and reproducible for repeated test cycles. The core/shell nanowires showed responses ranging from ~239 to ~619 %, whereas pristine SnO_2 and ZnO nanowires showed responses ranging from ~126 to ~180 % and from ~102 to ~104%, respectively, at NO_2 concentrations of 1–5 ppm (Table 1). Therefore, the responses of core/shell nanowires were 2–3- and 2–6-fold higher than those of pristine SnO_2 and ZnO nanowires, respectively.

Figure 6d shows the responses of pristine SnO_2 nanowires and SnO_2-core/ZnO-shell nanowires as a function of the NO_2 concentration under UV illumination. The response of an oxide semiconductor is commonly expressed as $R = A\ [C]^n + B$, where A and B are constants, and n and $[C]$ are the exponent and target gas concentration, respectively.[26] Data fitting provided the following equations: $R = 13.04\ [C] + 112.08$, $R = 0.57\ [C] + 100.95$, and $R = 92.07\ [C] + 132.59$ for pristine SnO_2 nanowires, pristine ZnO nanowires, and SnO_2-core/ZnO-shell nanowires, respectively. The response of SnO_2-core/ZnO-shell nanowires tended to increase more rapidly with increasing the NO_2 gas concentration than those of the two pristine nanowires, suggesting that the response of the former is far higher than those of the latter at high NO_2 gas concentrations, such as at a few thousand ppm of NO_2, even though the response of SnO_2-core/ZnO-shell nanowires was examined only over a NO_2 concentration range of 1–5 ppm.

Figure 7 shows the dynamic responses of SnO_2-core/ZnO-shell nanowires to 5 ppm NO_2 gas at room temperature under UV illumination at different intensities. The dynamic response of the core/shell nanowires at room temperature without UV illumination, i.e., for the UV intensity of 0 mW/cm^2, is not shown in Figure 7 because the change in resistance was unstable and negligible. The responses of the core/shell nanowires increased from 189% to 619% with increasing UV illumination intensity from 0.35 to 1.2 mW/cm^2 (Table 2). These high responses at room temperature highlight the strong influence of UV irradiation on the response of the nanosensor toward NO_2 gas. This result supports previous reports showing that a UV irradiation technique can be used to realize room temperature-gas sensors.[12−20]

The improvement in the response of the SnO_2 nanowires to NO_2 gas by encapsulating them with ZnO can be explained by the modulation of electron transfer by the n-SnO_2/n-ZnO heterojunction.[27] The surface states and/or defects on single crystalline nanowires can induce trap energy levels at the surfaces and interfaces, resulting in band bending due to Fermi level pinning.[28−30] The trapping of carrier electrons in the trap states can cause electron depletion in the surface and interface regions of the nanowires. On the other hand, the ZnO shell layer thickness (~10 nm) is smaller than the width of the surface depletion layer in the ZnO nanowires, which is the order of the Debye length of ZnO, ~30 nm[31,32] (Figure 8a,b). Consequently, the depletion region in the vicinity of the core/shell interface (SnO_2/ZnO heterojunction) overlaps the surface depletion region of the ZnO shell. In addition to the depletion regions, an energy barrier exists at the n-SnO_2/n-ZnO heterojunction due to electron trapping at the SnO_2-core/ZnO-shell interface as shown in Figure 8a. The energy barrier at the n–n heterojunction should also be considered when explaining the sensing mechanism of the core/shell nanowire sensors because electron transport is modulated by the heterojunction. The conductivity, σ, can be expressed as follows:[27]

$$\sigma = \sigma_0 \exp(\Phi_{eff}/kT) \quad (1)$$

where σ_0 is a constant, Φ_{eff} is the effective energy barrier at the n–n heterojunction, k is a Boltzmann constant, and T is the absolute temperature. Upon exposure to NO_2 gas, Φ_{eff} will increase because NO_2 gas is adsorbed by the core/shell nanowire and electrons are attracted to the adsorbed NO_2 molecules. Consequently, the electrical resistivity increases. On the other hand, after stopping the NO_2 gas supply, the electrons trapped by the adsorbed NO_2 molecules will be released and trapped not only by the ZnO shell layer but also by the SnO_2 core and n–n heterojunction. Φ_{eff} will decrease because the trapped electrons will return to the conduction band of ZnO. Consequently, the conductivity of the core/shell nanowire will increase or the resistivity will decrease. Therefore, electron transport is modulated by the n–n heterojunction with an adjustable energy barrier height.

Figure 8a presents the proposed mechanism for the enhanced NO_2 response of the SnO_2-core/ZnO-shell nanowire sensor under UV illumination. When the core/shell nanowire is exposed to air, it interacts with oxygen by transferring electrons from the conduction band to the adsorbed oxygen atoms, forming ionic species, such as O^-, O^{2-} and O_2^-, as shown in the following reactions:[30,33]

$$O_2\ (g) \rightarrow O_2\ (ads) \quad (2)$$

$$O_2\ (ads) + e^- \rightarrow O_2^-\ (ads) \quad (3)$$

$$O_2^-\ (ads) + e^- \rightarrow 2O^-\ (ads) \quad (4)$$

$$O^-\ (ads) + e^- \rightarrow O^{2-}\ (ads) \quad (5)$$

A depletion layer is created in the surface region of the core/shell nanowire due to the consumption of electrons in the surface region

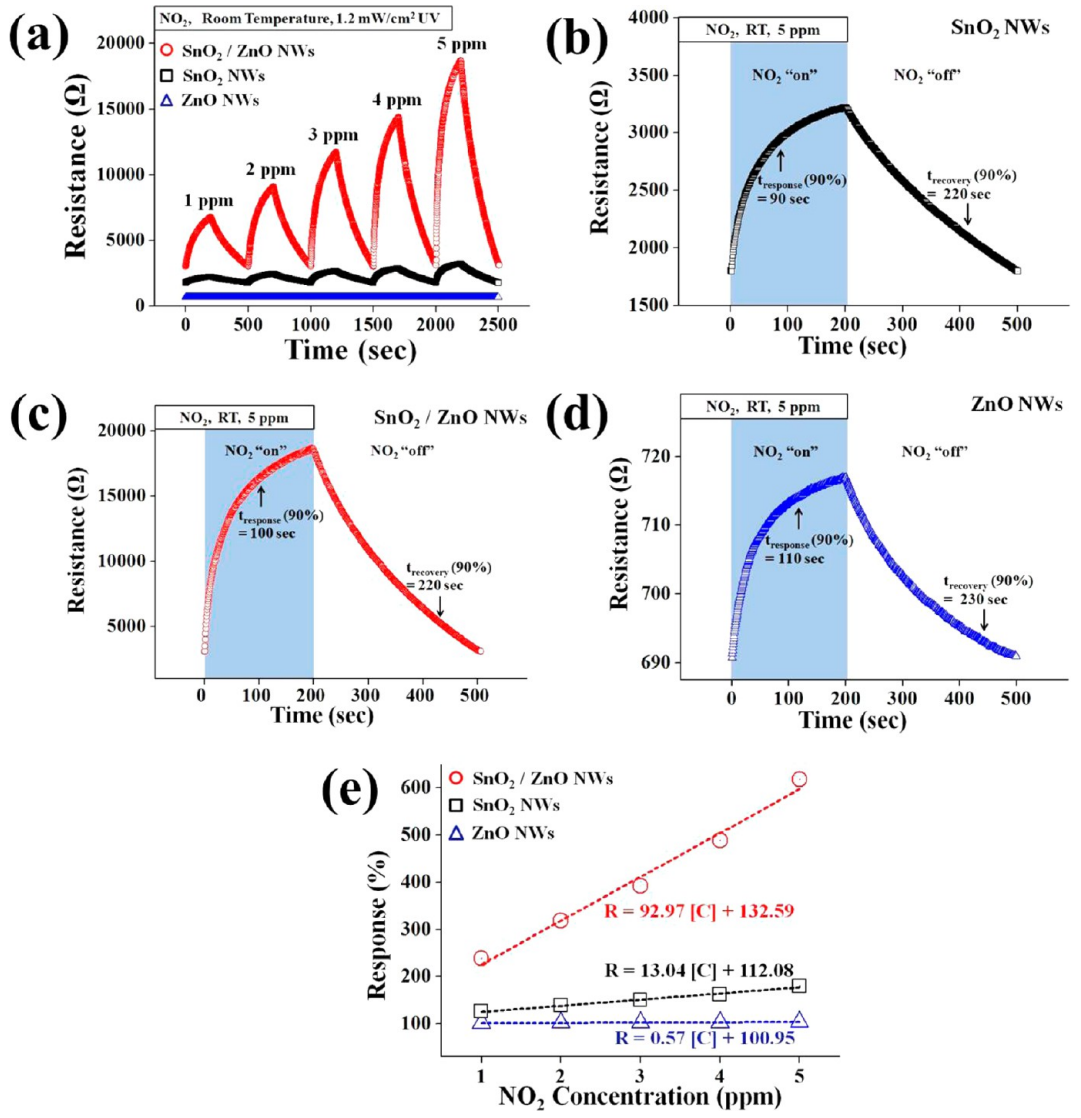

Figure 6. (a) Dynamic responses of pristine SnO_2 nanowire sensors, pristine ZnO nanowires, and SnO_2-core/ZnO-shell nanowires to NO_2 gas for the gas concentrations of 1−5 ppm at room temperature under UV illumination. (b) Enlarged part of (a): pristine SnO_2 nanowires at 5 ppm NO_2. (c) Enlarged part of (a): SnO_2-core/ZnO-shell nanowires at 5 ppm NO_2. (d) Enlarged part of (a): pristine ZnO nanowires at 5 ppm NO_2. (e) Responses of pristine SnO_2 nanowires and SnO_2-core/ZnO-shell nanowires as a function of the NO_2 gas concentration.

Table 1. Responses Measured at Different NO_2 Concentrations for Pristine SnO_2 Nanowires, Pristine ZnO Nanowires, and the SnO_2-Core/ZnO-Shell Nanowires at Room Temperature under UV Illumination at 1.2 mW/cm^2

	response (%)		
NO_2 conc. (ppm)	ZnO	SnO_2	SnO_2/ZnO
1	101.59	126.08	238.73
2	101.95	138.55	318.87
3	102.75	149.89	392.41
4	103.15	161.89	489.05
5	103.82	179.61	618.51

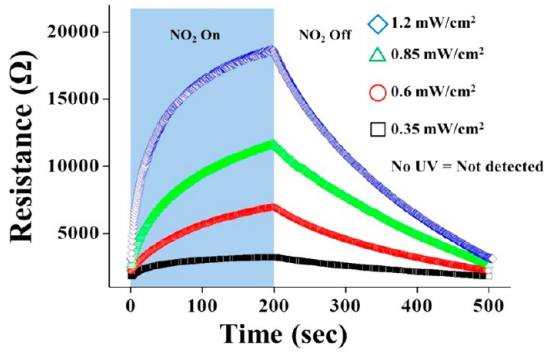

Figure 7. Dynamic responses of SnO_2-core/ZnO-shell nanowires to NO_2 gas at 5 ppm for different UV light illumination intensities.

of the core/shell nanowire. Electron-hole pairs will be generated in the ZnO shell upon exposure to UV light with a photon energy larger than the band gap of ZnO. On their way to the surfaces of the ZnO shell, some of the photo-generated electrons and holes will recombine with each other and many of the remaining photo-generated holes will react with negatively charged adsorbed oxygen ions on the surface according to the following reactions:[18]

$$h^+ (h\nu) + O^{2-} (ads) \rightarrow O_2 (g) \quad (6)$$

dx.doi.org/10.1021/am400500a | ACS Appl. Mater. Interfaces 2013, 5, 4285−4292

Table 2. Responses of SnO_2-Core/ZnO-Shell Nanowires to 5 ppm NO_2 Measured at Room Temperature for Different UV Illumination Intensities

UV power (mW/cm^2)	response (%)
0.35	188.69
0.6	323.29
0.85	455.84
1.2	618.51

$$h^+ (h\nu) + O^- (ads) \rightarrow 1/2O_2 (h\nu) \quad (7)$$

or

$$2h^+ (h\nu) + O^{2-} (ads) \rightarrow 1/2O_2 (h\nu) \quad (8)$$

As a result of these reactions, the surface depletion layer in the ZnO shell of each core/shell nanowire will be reduced.

Upon exposure to NO_2 gas, NO_2 gas adsorbs on the ZnO shells, and the remaining photo-generated electrons are released from the shells and are attracted to the adsorbed NO_2 molecules because an oxidizing gas, such as NO_2, acts as an electron acceptor, as shown in the following reaction:[15]

$$NO_2 (g) + e^- (h\nu) \rightarrow 2NO (h\nu) + O_2^- (h\nu) \quad (9)$$

This reaction widens the surface depletion region in the ZnO shell, resulting in an increase in the resistance of the nanowire sensor. Therefore, the depletion layer width and the electrical resistance of the sensor increase with increasing NO_2 concentration and UV illumination intensity due to an increase in the number of electrons participating in the above reactions. Electron transfer is modulated by the n-SnO_2/n-ZnO heterojunction under UV illumination as well as in the dark, because the surface depletion layer overlaps the interface depletion layer and W_D ($h\nu$) > W_D (dark) > 10 nm (ZnO shell layer width) (Figure 8b), where W_D ($h\nu$) and W_D (dark) represent the depletion layer width in the core/shell nanowire under UV illumination and in the dark, respectively. In other words, the n−n heterojunction acts as a lever in electron transfer through which electron transfer is facilitated or restrained, resulting in enhanced sensing properties of the core/shell nanowire sensor. On the other hand, after stopping the NO_2 gas supply, the resistivity will recover completely to the initial value due to the release of electrons trapped by the adsorbed NO_2 molecules in the same manner as in the dark.

Overall, the substantial improvement in the response of the core/shell nanowires to NO_2 gas by UV irradiation was attributed to the larger change in resistance caused by an increase in the

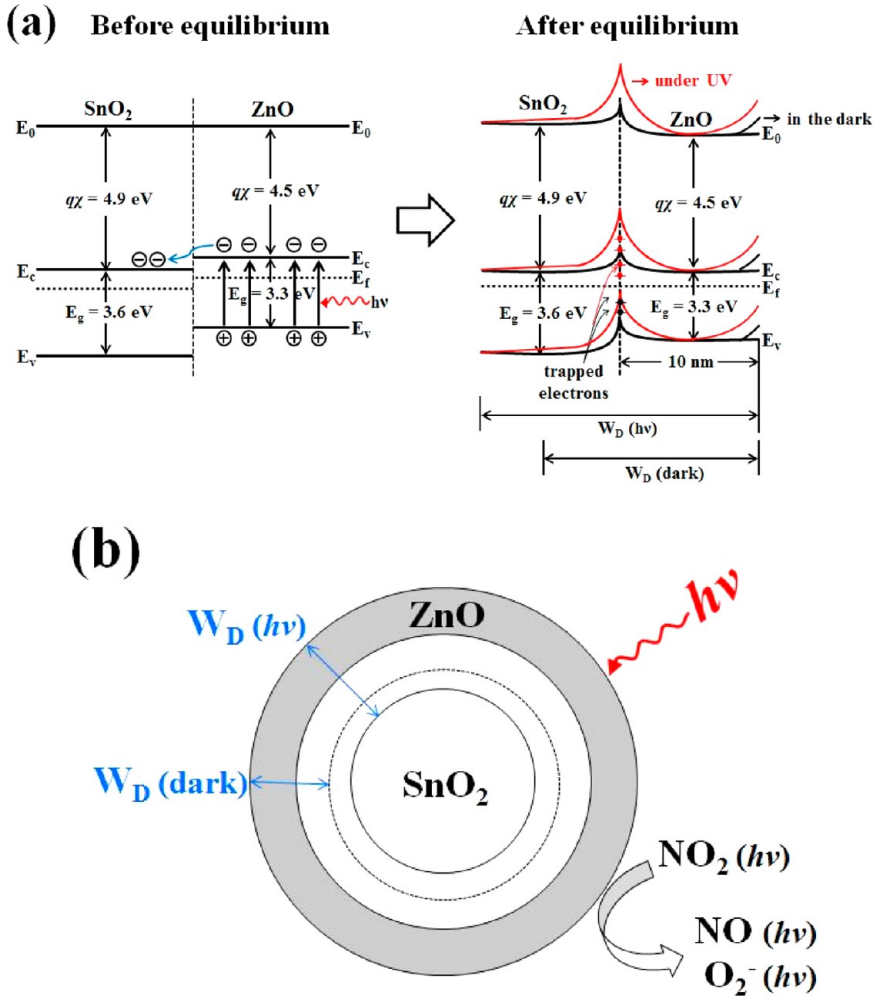

Figure 8. Schematic diagrams showing a mechanism proposed for the enhanced response of the SnO_2-core/ZnO-shell nanowire sensor to NO_2 under UV illumination: (a) Energy band diagram of the SnO_2/ZnO system. The red and black lines denote the cases with and without UV irradiation, respectively. (b) Cross-sectional view of the core/shell nanowire showing the reduction of the depletion region by UV irradiation. Figures are not drawn to scale.

number of electrons participating in the reactions with NO_2 molecules as a result of the photo-generated electron-hole pairs. The energy barrier at the heterojunction (Φ_{eff} in eq 1) is larger under UV illumination than in the dark and increases with increasing UV illumination intensity because more electrons are trapped by the heterojunction under UV illumination.

The interaction of SnO_2/ZnO-based sensors with NO_2 can be influenced by moisture.[34] In this study, NO_2 gas was designed to pass silica gel before it entered the sensing test chamber (Supporting Information, Figure S2) to minimize humidity compensation and heterogeneous adsorption of the surface due to the high and/or not constant humidity levels present in the environment and/or detected sample. On the other hand, the sensors do not necessarily guarantee work in real world conditions where humidity/temperature and fluctuations of humidity/temperature are critical because they work under ideal conditions.[35−37] Another issue not considered in this study is a hysteresis phenomenon. The electronic transport through the oxide NWs is affected by the periphery surfaces, interfaces, and/or adsorbed atmosphere molecules near the charge carrier channel. Generally, these interactive effects might lead to a hysteresis phenomenon, namely, a lag in the response.[38] Proper chemical passivation of the Zn−OH groups on the ZnO shell layer surface could serve to achieve stable and reproducible SnO_2/ZnO NW-based gas sensors under real-world humidity conditions.

4. CONCLUSIONS

SnO_2-core/ZnO-shell nanowires were synthesized using a two-step process: the synthesis of SnO_2 nanowires by the thermal evaporation of a mixture of Sn powders followed by the ALD of ZnO. The nanowires were 50−250 nm in diameter and up to a few to a few tens of μm in length. The cores and shells of the nanowires were single crystal SnO_2 and single crystal ZnO, respectively. The responses to NO_2 concentrations of 1 to 5 ppm ranged from 239% to 619%. Compared to those in pristine SnO_2 nanowires and pristine ZnO nanowires, the responses of the SnO_2-core/ZnO-shell nanowires were improved 2−3- and 2−6-fold, respectively, at NO_2 concentrations ranging from 1 to 5 ppm. This improvement in response can be explained by the modulation of electron transfer by the energy barrier at the SnO_2/ZnO heterojunction. On the other hand, the substantial improvement in the response of SnO_2 nanowires to NO_2 gas by UV irradiation was attributed to the increased change in resistance due to the photo-generation of electron-hole pairs.

■ ASSOCIATED CONTENT

Supporting Information

Distribution of the diameters of SnO_2 nanowires, ZnO nanowires, and SnO_2-core/ZnO-shell nanowires; schematic diagram showing the method to remove the moisture in the synthetic air used for sensing tests. This material is available free of charge via the Internet at http://pubs.acs.org.

■ AUTHOR INFORMATION

Corresponding Author

*Tel: +82 32 860 7536. Fax: +82 32 862 5546. E-mail: cmlee@inha.ac.kr.

Notes

The authors declare no competing financial interest.

■ ACKNOWLEDGMENTS

This study was supported by the Key Research Institute Program through the National Research Foundation of Korea (NRF) funded by the Ministry of Education, Science and Technology (2011-0018394).

■ REFERENCES

(1) Kolmakov, A.; Zhang, Y.; Cheng, G.; Moskovits, M. *Adv. Mater.* **2003**, *15*, 997−1000.
(2) Liu, Y.; Koep, E.; Liu, M. *Chem. Mater.* **2005**, *17*, 3997−4000.
(3) Law, M.; Kind, H.; Messer, B.; Kim, F.; Yang, P. *Angew. Chem., Int. Ed.* **2002**, *41*, 2405−2408.
(4) Park, S.; An, S.; Ko, H.; Jin, C.; Lee, C. *ACS Appl. Mater. Interfaces* **2012**, *4*, 3650−3656.
(5) Ramgir, N. S.; Mulla, I. S.; Vijayamohanan, K. P. *Sens. Actuators, B* **2005**, *107*, 708−715.
(6) Gundiah, G.; Govindaraj, A.; Rao, C. N. R. *Chem. Phys. Lett.* **2002**, *351*, 189−194.
(7) Gao, Y. H.; Bando, Y.; Sato, T.; Zhang, Y. F.; Gao, X. Q. *Appl. Phys. Lett.* **2002**, *81*, 2267−2269.
(8) Kim, H.; Jin, C.; Park, S.; Kim, S.; Lee, C. *Sens. Actuators, B* **2012**, *161*, 594−599.
(9) Arnold, S. P.; Prokes, S. M; Perkins, F. K.; Zaghloul, M. E. *Appl. Phys. Lett.* **2009**, *95*, 10312−10314.
(10) Choi, Y. J.; Hwang, I. S.; Park, J. G.; Choi, K. J.; Park, J. H.; Lee, J. H. *Nanotechnology* **2008**, *19*, 095508.
(11) Zhang, Y.; Kolmakov, A.; Lilach, Y.; Moskovits, M. J. *J. Phys. Chem.* **2005**, *109*, 1923−1929.
(12) Comini, E.; Cristalli, A.; Faglia, G.; Sberveglieri, G. *Sens. Actuators, B* **2000**, *65*, 260−263.
(13) Comini, E.; Faglia, G.; Sberveglieri, G. *Sens. Actuators, B* **2001**, *78*, 73−77.
(14) Prades, J. D.; Diaz, R. J.; Ramirez, F. H.; Barth, S.; Cirera, A.; Rodriguez, A. R.; Mathur, S.; Morante, J. R. *Sens. Actuators, B* **2009**, *140*, 337−341.
(15) Fan, S. W.; Srivastava, A. K.; Dravid, V. P. *Appl. Phys. Lett.* **2009**, *95*, 142106.
(16) Fan, S. W.; Srivastava, A. K.; Dravid, V. P. *Sens. Actuators, B* **2010**, *144*, 159−163.
(17) Gong, J.; Li, Y.; Chai, X.; Hu, Z.; Deng, Y. *J. Phys. Chem.* **2010**, *114*, 1293−1298.
(18) Cao, C.; Hu, C.; Wang, X.; Wang, S.; Tian, Y.; Zhang, H. *Sens. Actuators, B* **2011**, *156*, 114−119.
(19) Lupan, O.; Chow, L.; Chai, G. *Sens. Actuators, B* **2009**, *141*, 511−517.
(20) Lu, G.; Xu, J.; Sun, J.; Yu, Y.; Zhang, Y.; Liu, F. *Sens. Actuators, B* **2012**, *162*, 82−88.
(21) Yu, J. H.; Choi, G. M. *Sens. Actuators, B* **1998**, *52*, 251−256.
(22) Kim, H. W.; Kebede, M. A.; Kim, H. S. *Opt. Mater.* **2009**, *31*, 1853−1856.
(23) Park, J. Y.; Choi, S. W.; Kim, S. S. *J. Phys. D: Appl. Phys.* **2011**, *44*, 205403−205406.
(24) Pan, K. Y.; Lin, Y. H.; Lee, P. S.; Wu, J. M.; Shih, H. C. *J. Nanomater.* **2012**, *2012*, 279245−279250.
(25) Hwang, I. S.; Kim, S. J.; Choi, J. K.; Choi, J. W.; Ji, H. J.; Kim, G. T.; Cao, G.; Lee, J. H. *Sens. Actuators, B* **2010**, *148*, 595−600.
(26) Williams, D. E. *Solid State Gas Sensors*; Higler: Bristol, 1987.
(27) Weis, T.; Lipperheide, R.; Wille, U.; Brehme, S. *J. Appl. Phys.* **2002**, *92*, 1411−1418.
(28) Shalish, I.; Temkin, H.; Narayanamurti, V. *Phys. Rev. B* **2004**, *69*, 245401.
(29) Wang, D.; Seo, H. W.; Tin, C. C.; Bozack, M. J.; Williams, J. R.; Park, M.; Sathitsuksanoh, N.; Cheng, A. J.; Tzeng, Y. H. *J. Appl. Phys.* **2006**, *99*, 113509−113513.
(30) Liao, Z. M.; Zhang, H. Z.; Zhou, Y. B.; Xu, J.; Zhang, J. M.; Yu, D. P. *Phys. Lett. A* **2008**, *372*, 4505−4509.
(31) Barsan, N.; Weimar, U. *J. Electrochem.* **2001**, *7*, 143−167.

(32) Calarco, R.; Marso, M.; Richter, T.; Aykanat, A. I.; Meijers, R.; Hart, A. V. D.; Stoica, T.; Luth, H. *Nano Lett.* **2005**, *5*, 981−984.
(33) Yamazoe, N.; Sakai, G.; Shimanoe, K. *Catal. Surv. Asia* **2003**, *7*, 63−75.
(34) Paska, Y.; Stelzner, T.; Christiansen, S.; Haick, H. *ACS Nano* **2011**, *5*, 5620−5626.
(35) Tisch, U.; Haick, H. *MRS Bull.* **2010**, *35*, 797−803.
(36) Zilberman, Y.; Ionescu, R.; Feng, X.; Mullen, K.; Haick, H. *ACS Nano* **2011**, *5*, 6743−6753.
(37) Zilberman, Y.; Tisch, U.; Shuster, G.; Pisula, W.; Feng, X.; Mullen, K.; Haick, H. *Adv. Mater.* **2010**, *22*, 4317−4320.
(38) Paska, Y.; Haick, H. *ACS Appl. Mater. Interfaces* **2012**, *4*, 2604−2617.